Multiphoton lasing in atomic potassium: Steady-state and dynamic behavior

J. L. Font,[1] J. J. Fernández-Soler,[1] R. Vilaseca,[1] and Daniel J. Gauthier[2]
[1]*Departament de Física i Enginyeria Nuclear, Universitat Politècnica de Catalunya, Colom 11, E-08222 Terrassa, Spain*
[2]*Department of Physics, Duke University, Box 90305, Durham, North Carolina 27708, USA*
(Received 12 September 2005; published 21 December 2005)

We show theoretically that it is possible to generate laser light based on two-photon and other high-order multiphoton processes when an atomic beam of optically driven potassium atoms crosses a high-finesse optical cavity. We use a rigorous model that takes into account all the atomic substates involved in the optical interactions and is valid for any drive and lasing field intensities. The polarizations of the drive and lasing fields are assumed to be fixed. Stable and unstable laser emission branches are obtained, which are represented as a function of cavity detuning and are analyzed in terms of the fundamental quantum processes yielding them. Closed-curve laser-emission profiles are obtained for multiphoton lasing based on processes involving more than one lasing photon. Two-photon laser emission branches show relatively long segments of stationary emission, combined in general with some segments of nonstationary emission, or with segments of mixture with three-photon emission processes. Rayleigh and hyper-Rayleigh processes can become simultaneously resonant, entailing in such case a large and fast transfer of population from the atomic initial ground sublevel to other ground sublevels with different z components of the total angular momentum. They could be useful in generating multiphoton correlated field states. In all cases the largest laser emission intensities are obtained from the highest-order processes, rather than the lowest. These results open the way to the understanding of experiments performed in the past years and suggest possibilities for more efficient and varied types of multiphoton laser operation.

DOI: 10.1103/PhysRevA.72.063810 PACS number(s): 42.60.Lh, 42.50.Hz, 42.50.Gy

I. INTRODUCTION

Since the advent of the laser, there has been sustained interest in developing quantum oscillators that are based on higher-order stimulated emission processes, whereby n photons ($n \geqslant 2$) incident on an excited atom stimulate it to a lower energy state and n photons identical to the incident ones are added to the light beam. Such lasers are expected to display unusual behavior at both the quantum and classical regimes because the n-photon stimulated emission rate depends on the incident photon flux to the nth power, resulting in an inherently nonlinear light-matter interaction. One consequence of this nonlinear relation is that the unsaturated gain is proportional to the photon flux to the nth-1 power and thus the intracavity photon number undergoes a runaway process once the laser is brought above threshold (often with an injected trigger field), growing rapidly until the n-photon transition is saturated. Therefore, the laser operates in a highly saturated regime (a source of optical nonlinearity) even at the laser threshold, giving rise to the possibility that the laser will generate quantum states of the electromagnetic field and display dynamical instabilities. Most previous research has focused on two-photon lasers [1] because it is easier to achieve such lasing in experiments. The generalization to higher-order lasing was first studied theoretically in the 1970s [2], to the best of our knowledge, and has received sustained interest over the years [3–17].

In the optical part of the spectrum, there have only been three experimental realizations of two-photon lasers. One was based on a laser-pumped lithium vapor [18,19] and operated in the pulsed mode without the need for an optical resonator because the gain was so high. The other two were continuous-wave devices based on coherent driving of atoms contained in a high-finesse optical cavity. In these experiments, two-photon amplification occurred via stimulated scattering whereby two pump laser photons are destroyed and two new photons are added to the cavity mode during a stimulated emission event, what we denote as (2+2) laser emission. In one device, the amplification process can be best understood in terms of dressed atoms [1,20–24], while in the other it is easiest to understand its behavior in terms of a stimulated two-photon Raman process [1,25]. To our knowledge, there has been no report of higher-order ($n>2$) lasing. The main practical difficulty in achieving multiphoton lasing is the fact that the n-photon stimulated emission process is often overwhelmed by competing single-photon amplification or multiwave mixing processes.

There are two primary goals of this paper. One is to present a detailed theoretical study of the two-photon Raman laser [(2+2) lasing] described by Pfister *et al.* [25]. We take into account many of the complexities present in their experiment, including the coherent driving of the D_1 transition of ^{39}K atoms and all of the degenerate magnetic sublevels involved in the interaction. However, we only allow a fixed state of polarization of the beam generated by the laser and thus we cannot make predictions concerning the polarization instabilities they observed. Preliminary theoretical work along these lines has been presented in Ref. [26] using a highly simplified model of the atomic energy levels involved in the interaction.

The other goal is to describe the operating characteristics of a multiphoton laser that is also based on laser-driven ^{39}K atoms, but for a different cavity detuning in comparison to the two-photon Raman laser. The multiphoton laser simulta-

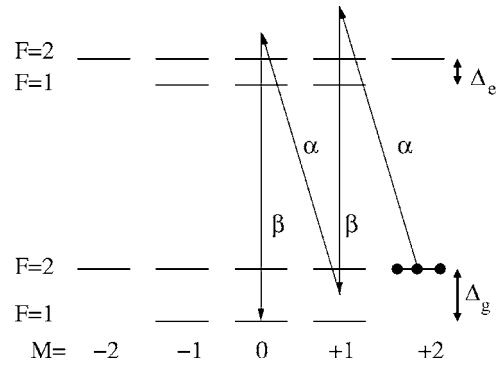

FIG. 1. Atomic energy levels for the ^{39}K D_1 transition, where $\Delta_g/\Lambda=37.43$ and $\Delta_e/\Lambda=4.677$. The atomic population is initially accumulated in atomic state $|g,2,2\rangle$. The arrows represent the two drive (α) photons and two probe or lasing (β) photons involved in the (2+2) process.

neously supports frequency-degenerate one-through four-photon lasing as well as stepwise (or cascade) lasing by combination of the underlying stimulated emission processes, denoted by $\Sigma_n(n+n)$ lasing. This system represents the first practical method for achieving frequency-degenerate multiphoton lasing in the optical part of the spectrum.

This paper primarily focuses on the characteristics of multiphoton laser emission from the laser-driven system. It is an extension of our previous paper, where we described both multiphoton amplification and lasing in a simplified atomic system that consisted only of a subset of the degenerate magnetic sublevels of the ^{39}K D_1 transition [27], and of an extended discussion of the multiphoton amplification process [28]. There exists an interesting variety of multiphoton processes that can occur in this system, where, for example, the (2+2) process is shown schematically in Fig. 1. We describe these interactions using a semiclassical density-matrix approach, where the atoms are treated quantum mechanically and the electromagnetic fields are treated classically.

The organization of this paper is as follows. We describe our model of the laser in the next section, describe the operating characteristics of the (2+2) and $\Sigma_n(n+n)$ laser in the following section, and end with some brief conclusions.

II. MODEL

Based on the experimental arrangement used by Pfister *et al.* [25], we consider an atomic beam of ^{39}K propagating in the x direction, although our theoretical model can be applied to any alkali-metal atom provided its nuclear spin is $I=3/2$. In the experiment described in [25], the atoms are first optically pumped into the initial state $|g,2,2\rangle$ by means of two $\hat{\sigma}_+$ polarized fields, thus creating the necessary population inversion for multiphoton transitions starting from $|g,2,2\rangle$. The atomic states are denoted by $|(g,e),F,M\rangle$, where g or e denote a state belonging to the ground or excited level manifold, respectively (see Fig. 1), and F and M denote the quantum numbers associated to the total angular momentum of the atom and its projection on axis z, respectively (the possible values of F are 1 and 2, for both the ground-or excited-level manifolds). The preparation of atoms in specific states is described in our model by means of a set of incoherent pumping rates, one for each state in the ground-level manifold. Each one of these parameters gives the rate of atoms in a specific state entering the interaction zone. According to the efficiency of the atomic state preparation reported by [29], we assume that about 93% of the atoms are in the $|g,2,2\rangle$ state just before entering the interaction region. The rest of the atoms are assumed to be distributed uniformly over the rest of states in the ground-level manifold.

The atoms interact with a plane-wave $\hat{\sigma}_-$ polarized drive field of the form

$$\hat{E}_d(z,t)=[\hat{e}_- E_d \exp\{i(k_d z-\omega_d t)\}+\text{c.c.}]/2 \tag{1}$$

propagating in the z direction, with fixed amplitude, wave number, and frequency E_d, k_d, and ω_d, respectively. The drive field only couples with transitions $|g,F,M\rangle \leftrightarrow |e,F',M-1\rangle$ for any allowed value of F, F', and M. The generated lasing field is described by a plane-wave $\hat{z}$-polarized field which reads

$$\hat{E}_L(y,t)=[\hat{e}_z E_L \exp\{i(k_L y-\omega_L t-\varphi_L)\}+\text{c.c.}]/2 \tag{2}$$

propagating in the y direction, with amplitude, wave number, and frequency E_L, k_L, and $\omega_L+\dot{\varphi}_L$, respectively (φ_L denotes the instantaneous phase of the laser field). Thus, we assume that the optical cavity axis is along the y direction, and that the atoms (or the atomic beam) enter an intracavity region where they interact simultaneously with the drive and the generated laser fields. Although the experiments [25] used a Fabry-Perot cavity, we consider here a ring configuration with a unidirectional traveling-wave lasing field for simplicity. The lasing field only interacts with transitions $|e,F,M\rangle \leftrightarrow |g,F',M\rangle$. The corresponding Rabi frequencies for each transition and these two fields are given by

$$2\alpha_{ij}=\frac{\mu_{ij}E_d}{\hbar}, \quad 2\beta_{ij}=\frac{\mu_{ij}E_L}{\hbar}, \tag{3}$$

where $\mu_{ij}=\mu_0\chi_{ij}$ represents the electric-dipole matrix element for a transition between atomic states i and j and the dimensionless parameter χ_{ij} is given by the corresponding Clebsch-Gordan coefficient. The values of both factors μ_0 and χ_{ij} are given in Ref. [28]. Whenever necessary, averaged values $2\alpha=\mu_0 E_\text{d}/\hbar$ and $2\beta=\mu_0 E_\text{L}/\hbar$ for the drive and laser field frequencies are used. Since laser emission can be nonstationary (i.e., time dependent), the laser half Rabi frequencies β_{ij} (or β) and frequency $\omega_L+\dot{\varphi}_L$ will in general be assumed to be time dependent. Concerning the laser frequency, if ω_L is taken to be constant and equal to the frequency of the closest empty-cavity mode, the time variations will only affect $\dot{\varphi}_L$. This last quantity, on the other hand (as is well known in laser physics), will represent the "frequency pushing or pulling" effect brought about by the change in the refractive index of the laser medium induced by the interaction of the laser field with the atoms.

The semiclassical density-matrix equations describing the evolution of the laser system in the usual rotating-wave, slowly varying envelope, and uniform-field approximation [30–32] can be expressed as

$$\dot{\rho}_{ii}(t) = \lambda_i - \left[\sum_j \gamma_{ji} + \gamma_{out}\right]\rho_{ii}(t) + \sum_j \gamma_{ij}\rho_{jj}(t) + \mathcal{F}_{ii}\{\rho_{ij}(t), \beta_{ij}(t); \alpha_{ij}, \Delta_d, \Delta_c\},$$

$$\dot{\rho}_{ij}(t) = -\Gamma_{ij}\rho_{ij}(t) - \mathcal{F}_{ij}\{\rho_{ii}(t), \rho_{jj}(t), \beta_{ij}(t); \alpha_{ij}, \Delta_d, \Delta_c\},$$

$$\dot{\beta} = -\beta(\kappa + \mathrm{Im}\,\tilde{G}), \quad \dot{\varphi}_L = -\mathrm{Re}\,\tilde{G}, \tag{4}$$

where the first two equations describe the atomic state evolution and the last two equations describe the laser field evolution. In the first two equations, ρ_{ii} stands for the population of state $i \equiv |n, F, M\rangle$ (with n being e, excited, or g, ground) and ρ_{ij} stands for the slowly varying envelope of the atomic coherence induced on the transition between states i and j. The rate of the injection of atoms with internal state i into the region of interaction with the fields is given by λ_i. The parameter γ_{out} gives the rate at which the atoms leave the interaction zone and is equal to the inverse of the average interaction time of the atoms with the fields. Since the system is closed, $\Sigma_i \lambda_i = \gamma_{out}$. Population relaxation rates from state j to i, denoted by γ_{ij}, are determined using the standard formula for the Einstein coefficient; thereby $\gamma_{ij} = \Lambda|\chi_{ij}\rangle^2$, where $\Lambda = (16\pi^3\mu_0^2)/(3h\epsilon_0\lambda^3)$ [28]. Since the effect of collisions among atoms on the coherence relaxation rates have been neglected, relaxation of the coherence $\rho_{ij}(t)$ is given by $\Gamma_{ij} = \gamma_{out} + (\Sigma_k \gamma_{ki} + \Sigma_k \gamma_{kj})/2$.

The functions $\mathcal{F}_{ii}$ and $\mathcal{F}_{ij}$ in Eq. (4) represent the interaction between the fields and the amplifying medium [28]. They exhibit the nonlinear character inherent to the interaction between radiation and matter. The parameter Δ_d that appears in these functions is defined as the difference between the driving field frequency ω_d and the frequency of the atomic transition between the excited $F=2$ and the ground $F=1$ levels (Fig. 1), which is taken as a reference frequency. The parameter Δ_c represents the cavity detuning and, in order to facilitate physical interpretation of the numerical results, has been defined as the difference between the closest empty-cavity eigenmode frequency and the drive field frequency.

Concerning the laser field, the third equation of (4) describes the evolution of the slowly varying envelope of the laser Rabi frequency 2β. The first term describes the field attenuation due to cavity losses, which, in the uniform-field limit, are assumed to be distributed uniformly along the cavity axis (κ represents the cavity loss rate). The second term describes the field amplification, where the generalized complex gain is given by

$$\tilde{G} = \frac{g}{\beta}\sum_{F,F'}\sum_M \chi_{gF'M,eFM}\rho_{eFM,gF'M}, \tag{5}$$

where the summation extends to all one-photon atomic coherences induced on the transitions $|e, F, M\rangle \rightarrow |g, F', M\rangle$, the unsaturated gain parameter is denoted by $g = N\omega_L\mu_0^2/(2\epsilon_0\hbar)$, and N is the density of atoms in the interaction region.

Finally, the last equation of (4) gives the frequency pushing effect, which determines the laser frequency. Note that this equation is decoupled from the others because $\dot{\varphi}_L$ does not appear explicitly in them.

Throughout the next section all quantities are expressed in dimensionless form by dividing all frequencies by Λ defined above, and, in a consistent manner, time has been multiplied by Λ and g has been divided by Λ^2.

III. RESULTS

In this section we present the results of the numerical integration of coupled equations (4). As pointed out in the Introduction, our operating conditions for the laser system will try to imitate, as closely as possible, the experimental conditions of [25], except for the fact that our model only allows for fixed polarization of the generated laser field. Our scope, on the other hand, will be larger than that of the experiments of [25]; we consider larger ranges of physically attainable laser parameters and we will consider other possibilities of multiphoton laser emission in the system.

In our study, we have used two complementary strategies for evaluating Eqs. (4).

Strategy (i). This strategy consists of integrating only the two first equations of (4), for fixed and constant values for the laser field amplitude β and frequency (independent of the values of the cavity detuning and losses). This allows us to calculate $\tilde{G}$, where $\mathrm{Im}\,\tilde{G}$ gives the relative increase in the probe-field amplitude per unit of time, whereas $-\mathrm{Re}\,\tilde{G}/\omega_L$ is proportional to refractive index change of the laser medium at the laser field frequency, brought about by the action of the drive and lasing fields [28].

Having determined $\tilde{G}$ and imposing the well-known conditions in laser physics for *stationary* laser emission, namely $\mathrm{Im}\,\tilde{G} = \kappa$ (gain factor=cavity losses) and $\mathrm{Re}\,\tilde{G} = -\dot{\varphi}_L$ (frequency pushing and/or pulling effect), it is possible to obtain the stationary solutions of the laser system, be them stable or *unstable*, as illustrated below.

Strategy (ii). The second strategy consists of integrating all the coupled equations in (4). In this case, the laser field amplitude and frequency are variables of the system. This method gives the stationary solutions, but only when they are *stable*, and also gives (when the stationary solutions are unstable) the time-dependent solutions.

Combining these two strategies allows us to completely characterize the laser system emission states.

We start with Fig. 2, which shows a panoramic view of the whole gain or lasing emission spectrum, including all the resonances due to different multiphoton processes. Figure 2(a) has been calculated following strategy (i) above, whereas Fig. 2(b) has been calculated following strategy (ii). In Fig. 2(a) the continuous line shows the gain peaks corresponding to different multiphoton processes as a function of the laser field frequency for fixed values of the drive and laser field amplitudes. Such laser field frequency is described, in the abscissa axis of Fig. 2(a), by means of a detuning Δ_L, which expresses the difference between the laser-field frequency and the drive-field frequency. The dif-

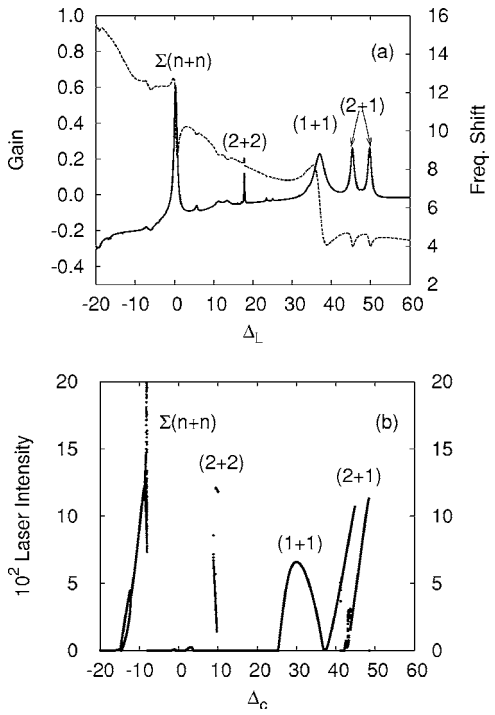

FIG. 2. Lasing characteristics of the laser-driven potassium atoms contained in a high-finesse optical resonator. (a) Gain factor $\mathrm{Im}\,\tilde{G}$ (left scale, solid line) and frequency shift $\dot{\varphi}_L$ (right scale, dashed line) as a function of laser field detuning Δ_L for a drive amplitude $\alpha=12$ and a laser field amplitude $\beta=15$. Other parameters: drive detuning $\Delta_d=4.86$, $\gamma_{out}=0.07$, $g=3000$, and 93% initial population of the atomic state $|g,2,2\rangle$. (b) Laser intensity β^2 (in hundreds) vs cavity detuning Δ_c for cavity losses $\kappa=0.05$; the rest of parameters are as in (a), except for the fact that β is a laser equation variable rather than a parameter.

ferent multiphoton processes have been labeled, as in [28], as $(n+m)$, where n represents the number of absorbed drive photons and m the number of emitted laser photons [absorption of drive photons and emission of laser photons occur in an alternate way, as in the example depicted in Fig. 1 corresponding to the (2+2) process]. Most of these multiphoton processes, in particular those that have been labeled in Fig. 2(a), start at the initially most populated state $|g,2,2\rangle$ (Fig. 1).

The properties of these multiphoton gain resonances have been analyzed in detail in [28], and thus will not be reproduced here. Instead, we will focus on the problem of determining the laser spectral emission profile; i.e., the laser emission intensity as a function of the cavity detuning. To this end, Fig. 2(a) also shows the frequency shift $\dot{\varphi}_L \equiv -\mathrm{Re}\,\tilde{G}$ (dashed line). The fact that this frequency shift is positive indicates that we are in the presence of frequency pushing. This is opposite to what occurs in the case of standard homogeneously broadened two-level lasers, where there is frequency pulling. This means that the cavity detuning Δ_c will be smaller than the laser field detuning Δ_L, since $\Delta_c=\Delta_L-\dot{\varphi}_L$. Such pushing occurs because of the proximity of the strong absorption resonance appearing near $\Delta_L=-40$ [28], which is associated with transitions $|g,2,M\rangle \rightarrow |e,2,M\rangle$ for any value of M (the largest contribution coming from the case $M=2$). The value of the frequency shift depends on the value of Δ_L, ranging, over the region of the appearance of the multiphoton gain peaks [Fig. 2(a)], from ~4 to 13.

Figure 2(b) is obtained following strategy (ii), which shows the stable or time-dependent laser emission intensity (defined as β^2) as a function of Δ_c, for the same drive field amplitude as in the previous subfigure and with $\kappa=0.05$. Comparison between Figs. 2(b) and 2(a) shows that the strong frequency pushing effect pointed out above strongly redshifts all the gain resonances. It is also seen that most gain resonances become strongly distorted: only fragments of branches appear, which means that the emission is unstable for the missing fragments, and thus only time-dependent or zero-intensity solutions are possible there. Time-dependent solutions can be distinguished in Fig. 2(b) by the fact that two curves have been plotted instead of a single one. One curve (the highest one) gives the maxima intensity values reached during the time evolution and the other curve (the lowest one) gives the minima intensity values [such time-dependent behavior can be clearly seen, for instance, over parts of the emission profile corresponding to the process $\Sigma_n(n+n)$, which will be analyzed later].

The sharp (and surprising) contrast between the shape of the resonances in Figs. 2(a) and 2(b) needs to be investigated in more detail. To this end, we next analyze separately each multiphoton laser emission resonance, starting by (and paying most attention to) the (2+2) process, which corresponds to the "two-photon" process investigated experimentally in Refs. [25,29]. We will also focus on the resonant "hyper-Rayleigh" process $\Sigma_n(n+n)$.

A. (2+2) multiphoton laser emission

Figures 3 and 4 are similar to Fig. 2(a), but with a narrower domain of cavity detunings considered so that only the gain feature corresponding to the (2+2) multiphoton process is evident. In the figures, each curve corresponds to a different value of the laser field amplitude β used in our strategy (i). The apparent change in the position and strength of the gain peaks when β is increased was already predicted and analyzed in [28]. Note, in particular, that the gain increases when the field amplitude β is increased, corresponding to a second-order process on that field. Such an increase, however, becomes saturated at large field amplitudes. The feature that was not observed in [28] is the progressive emergence of an extra peak (appearing at the left-hand side of the main peak) as β increases. This peak corresponds to a (4+3) multiphoton process, which was not detected in [28] because such a process ends on state $|e,2,-2\rangle$ and hence was ignored in numerical code used in that work. The position of such (4+3) resonance, for low drive and laser field amplitudes, is at $\Delta_L=(\Delta_g+\Delta_e)/3$ (=14.10 in the example considered in our figures), but the lightshifts of the initial and final atomic states for that process, induced by the drive and laser fields, blueshift the resonance so that it appears quite close to the (2+2) resonance (whose unshifted position is at $\Delta_L=\Delta_g/2=18.72$ and the light fields make it to redshift, as analyzed in [28]). The question arises whether this (4+3) resonance could contaminate the (2+2) lasing for large laser emission

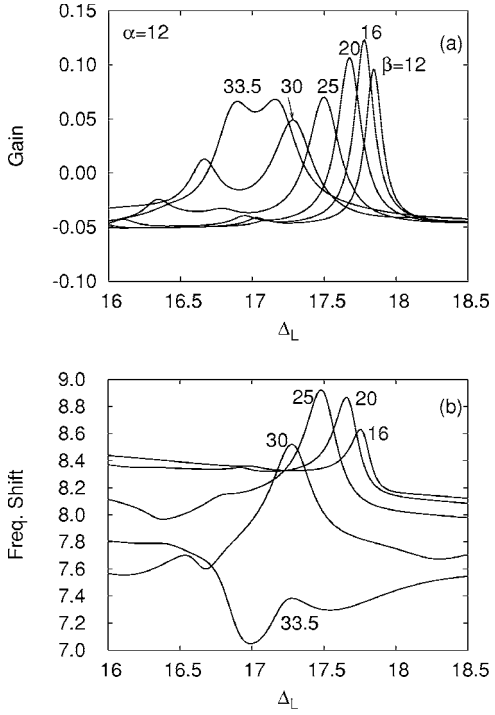

FIG. 3. Two-photon lasing characteristics of laser-driven potassium atoms contained in a high-finesse optical resonator. Gain Im $\tilde{G}$ (a) and frequency shift $\dot{\varphi}_L$ (b) as a function of the laser detuning Δ_L for $\alpha=12$ and several probe amplitudes. The rest of parameters are the same as in Fig. 2(a).

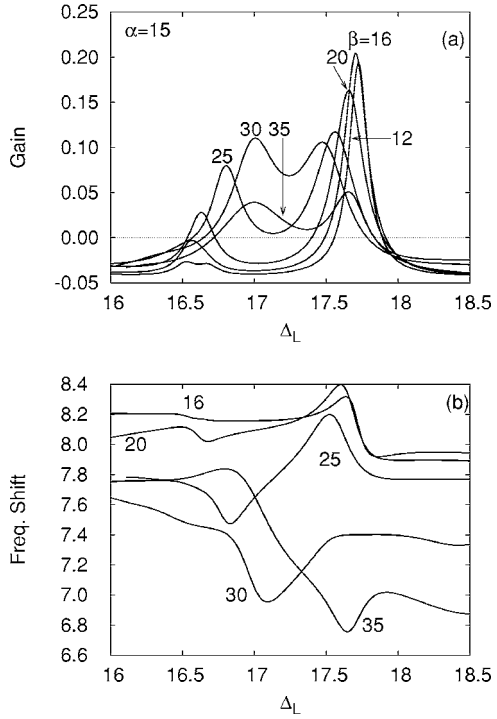

FIG. 4. Two-photon lasing characteristics of laser-driven potassium atoms contained in a high-finesse optical resonator. Gain Im $\tilde{G}$ (a) and frequency shift $\dot{\varphi}_L$ (b) as a function of the laser detuning Δ_L for $\alpha=15$ and several probe amplitudes. The rest of parameters are the same as in Fig. 2(a).

intensities; this point will be discussed below.

Figures 3(b) and 4(b) show the frequency pushing effect $\dot{\varphi}_L$ corresponding to each of the curves of Figs. 3(a) and 4(a). The shape corresponds approximately to a broadened dispersive profile, which is distorted by the dispersivelike structure associated with the (4+3) processes at large field amplitudes β.

From these figures, it is possible to calculate the corresponding laser emission profile for stationary emission in the following way. Draw a horizontal straight line over Fig. 3(a) or 4(a) that crosses the vertical axis at a value equal to the cavity loss rate κ. The working point of the laser is determined by imposing lasing condition ["gain=loss," as pointed out above when describing strategy (i)] and corresponds to the intersection of this line with the appropriate gain curve for each value of Δ_L. In this way, the laser emission profiles depicted in Figs. 5(a) and 7(a) are obtained. These laser emission profiles are given as a function of the laser field detuning Δ_L. If we now take into account the frequency shifts $\dot{\varphi}_L$ described by Figs. 3(b) and 4(b), the laser emission profile can be finally depicted as a function of the cavity detuning Δ_c, as shown in Figs. 5(b) and 7(b).

Let us now analyze the results of Figs. 5(a) and 5(b). Each figure shows the emission profiles for $\kappa=0.10$ (inner closed curve) and $\kappa=0.05$ (the two other, larger size, closed curves). For $\kappa=0.10$, a smooth closed curve is obtained, in both Figs. 5(a) and 5(b). Careful comparison with Fig. 3(a) shows that, in this case, only the (2+2) multiphoton process contributes to laser emission with no participation of the (4+3) or other processes. We can thus affirm that we are in the presence of pure "two-photon" emission. The shape of the emission profile in Fig. 5(a), with such a closed curve, is in sharp contrast to the case of a standard single-photon laser, where the emission profile consists of a symmetric peak connecting on both wings with the zero-intensity branch. This implies that the zero-intensity solution is stable for (2+2) lasing, and the two-photon lasing emission must necessarily be triggered with an initial signal. Such emission profile in the form of a smooth closed curve and the associated need for initial triggering are in qualitative agreement with the predictions of simple models of two-photon lasers based on two-or three-level schemes [1,33], although the quantitative details of the emission profile are different.

It must be pointed out here that the procedure outlined above to obtain the emission profiles of Figs. 5(a) and 7(a), which is based on strategy (i), does not allow us to determine the stability of the branches. The stable parts of each branch have been determined using strategy (ii). Such stable parts have been plotted, in Figs. 5(a) and 7(a), using large dots. Note that these thick-line segments perfectly match the underlying curves obtained using strategy (i). In the case of Fig. 5 with $\kappa=0.10$, it can be seen that the stable part of the emission profile corresponds with the upper part of the closed curve giving the stationary emission.

For the case of smaller cavity losses ($\kappa=0.05$), Fig. 5(a) shows that the emission profile continues to be in the form of a closed curve, but of a larger size than in the previous case. The emission corresponding to this curve continues to corre-

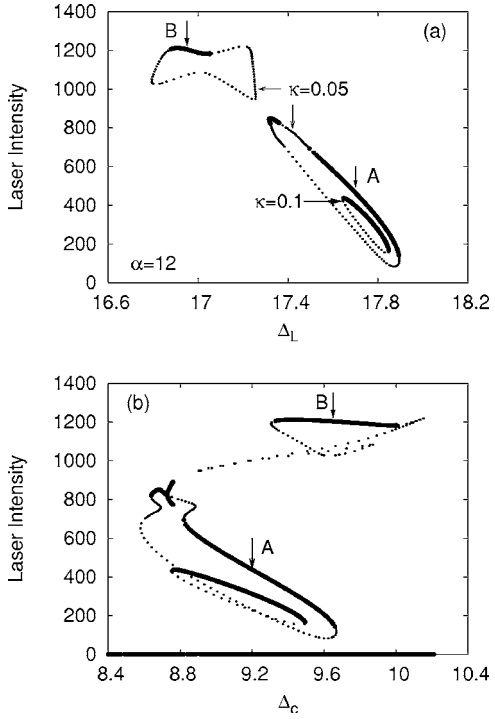

FIG. 5. Two-photon lasing characteristics of laser-driven potassium atoms contained in a high-finesse optical resonator. (a) Laser intensity β^2 vs laser field detuning Δ_L for $\alpha=12$ [the rest of parameters as in Fig. 2(a)]. The inner (smaller) oval is for cavity losses $\kappa=0.10$; the two other (larger size) ovals are for $\kappa=0.05$. The small dots correspond to the predictions following strategy (i) representing all possible stationary (both stable and unstable) emission states. The large dots correspond to the predictions following strategy (ii) and thus represent all the possible stable emission states. (b) The same as in (a), except as a function of the cavity detuning Δ_c. In (b), time-dependent (periodic) behavior has also been included; in such cases the maximum and minimum intensity values reached by the laser intensity along time evolution have been plotted. Points labeled *A* and *B* are discussed in the text.

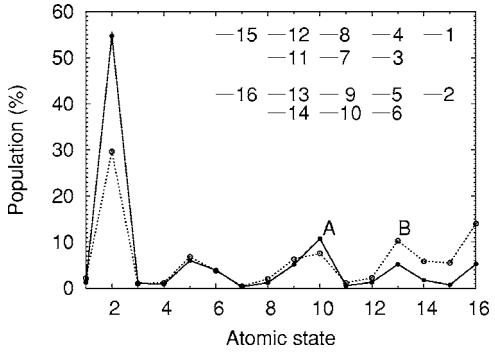

FIG. 6. Population (as a percentage) reached by each atomic state during stable laser emission for the conditions indicated by the two points *A* (black circles and solid line) and *B* (open circles and dashed line) of 5(b) The inset shows the simplified notation used for the atomic states (compare with 1). The manifold $|e,2,M\rangle$ corresponds to levels 1, 4, 8, 12, and 15 in decreasing M order; $|e,1,M\rangle$ corresponds to levels 3, 7, and 11; $|g,2,M\rangle$ corresponds to levels 2, 5, 9, 13, and 16; and $|g,1,M\rangle$ corresponds to levels 6, 10 and 14.

spond to the (2+2) multiphoton emission process. A feature is the second closed curve appearing at the top left of the figure. Careful comparison with Fig. 3(a) shows that this closed curve corresponds to the (4+3) multiphoton process and its mixture with the (2+2) process. The emission intensity for this closed curve is larger than in the case of the other closed curve. It must be pointed out that, for the closed curve corresponding to the (2+2) process, there is a slight contamination by the (4+3) process at the points closest to the curve corresponding to the (4+3) process (i.e., at the top left corner of the closed curve).

When looking now at the same case ($\kappa=0.05$) but in Fig. 5(b), it is seen that the frequency-pushing effect strongly distorts the closed curve containing the (4+3) processes, because of its inhomogeneity [as shown in Fig. 3(b)]. In contrast, distortion of the other closed curve [i.e., the one corresponding to the (2+2) processes] is significant only at its highest-intensity part (where it is closest to the other curve); such distortion is the only effect of the (4+3) processes on that curve. Concerning stability, it can be seen in Fig. 5(b) that there is a relatively long segment of stable emission that corresponds essentially to (2+2) processes [(bottom curve with $\kappa=0.05$, segment going from $\Delta_c=8.9$ to 9.7), and also a small segment of stable emission at the top of the closed curve (near $\Delta_c=8.7$), which thus lies in the region where there is some contamination with (4+3) processes. Note that this last segment of stable emission connects, on its right-hand end, with a narrow domain of periodic emission (time-dependent emission has been calculated following strategy (ii)]. All these segments appear at different values of the cavity detuning, so that they can be addressed separately. It is also worth pointing out that there is tristability between the zero-intensity solution, the (2+2) solution, and the mixed (4+3) and (2+2) solutions in the domain $\Delta_c=9.3$ to 9.7. In practice, they can be distinguished by the different levels of emission intensity they sustain. Finally, the segments of stable or periodic emission in Fig. 5(b) are no other than those appearing in Fig. 2(b) for the region between $\Delta_c=8$ and 10.

Figure 6 shows the populations of each of the atomic states for two specific points (or laser emission states) of the stable branches depicted in Fig. 5(b). The black circles and solid line correspond to the case of a pure (2+2) process [point *A* of Fig. 5(b)], while the open circle and dashed line correspond to the case of mixed (4+3) and (2+2) processes [point *B* of Fig. 5(b)]. For the two (2+2) processes, it is seen that the atomic population is effectively transferred from the initial state $2\equiv|g,2,2\rangle$ to, predominantly, the atomic state $10\equiv|g,1,0\rangle$, which is the final state of the (2+2) multiphoton process. Some population appears in the other states via other multiphoton processes or through spontaneous emission from the excited atomic states. In contrast, in the mixed (4+3) and (2+2) case, population is transferred not only to these states but also, in a large amount, to the state $15\equiv|e,2,-2\rangle$ which is the final atomic state for the (4+3) process. Note, however, that this final atomic state is an excited state so that population decays from that state and accumulates in the directly accessible ground states $13\equiv|g,2,-1\rangle$,

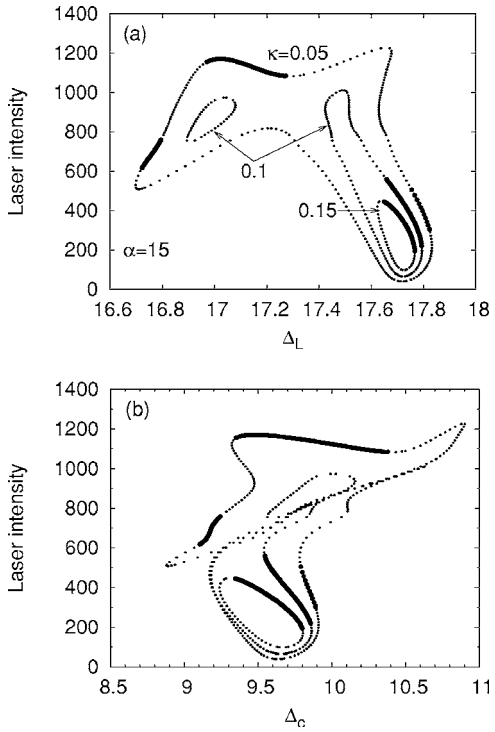

FIG. 7. The same as in Fig. 5, but for a larger drive amplitude of $\alpha=15$ and cavity losses of $\kappa=0.05$ [outer closed curve in (a)]; $\kappa=0.10$ (intermediate closed curves), and $\kappa=0.15$ (inner closed curve).

$14\equiv|g,1,-1\rangle$, and $16\equiv|g,2,-2\rangle$. Note, in particular, the large amount of population that is transferred to the "extreme" ground state $16\equiv|g,2,-2\rangle$.

Figure 7 is similar to Figs. 5(a) and 5(b) for the case when the drive field is larger ($\alpha=15$). In this situation, laser emission exists for a larger domain of cavity losses, where we now show three different values of the cavity loss rate. The predicted behaviors are similar as in the previous case described above. Looking first at Fig. 7(a) for large cavity losses ($\kappa=0.15$), a single smooth closed curve is obtained (see the inner most curve) whose upper branch is stable. For moderate cavity losses ($\kappa=0.10$), two closed curves appear, one for (2+2) multiphoton processes and another for (2+2) and (4+3) processes (as in Fig. 5). For the smallest cavity losses ($\kappa=0.05$), the two closed curves merge together because of the strong mixture and coupling between the two processes. From Fig. 7(b), it is seen that the pushing effects again strongly distort the laser emission profile, except in the case of the largest cavity losses.

The general conclusion that can be drawn from Figs. 5 and 7, as well as from other calculations not reported here for the sake of brevity, is the laser stationary emission profile is essentially in the form of a smooth closed curve (oval type) whose upper branch is stable and corresponds to (2+2) multiphoton processes for low or moderate drive amplitudes or for large cavity losses, where the lasing field intensity is moderate and thus nonlinear effects are weaker. This is the case, for instance, when $\alpha=12$ and $\kappa=0.10$ or when $\alpha=10$ and $\kappa=0.05$. In contrast, for large drive amplitude and/or small cavity losses, the influence of (4+3) multiphoton processes strongly distorts the stationary emission profile of the laser. In this last case, stable emission occurs only over pieces of the stationary emission branches; there also exists segments corresponding to pure (2+2) emission processes. Finally, there are also pieces of branch where emission is nonstationary and thus giving rise to time-dependent behavior.

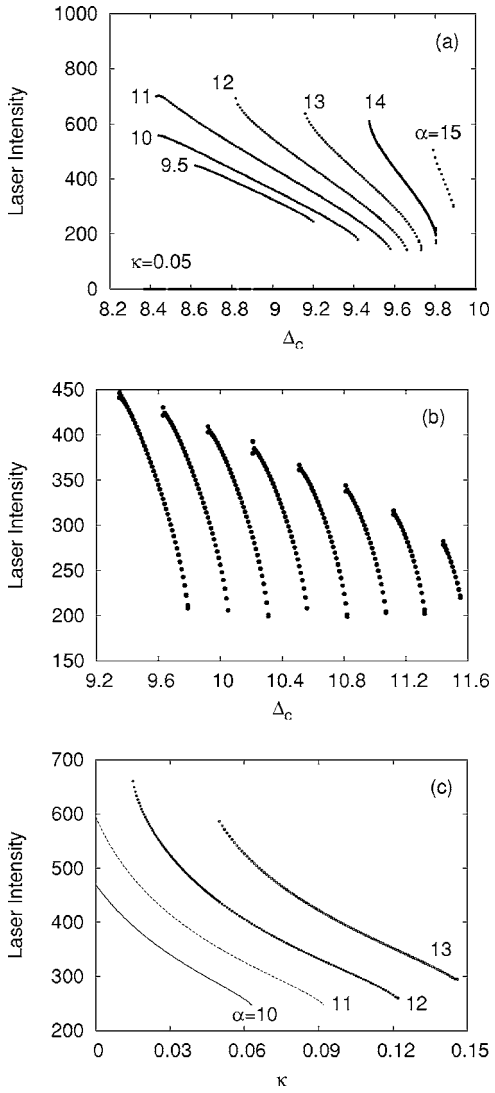

FIG. 8. Two-photon lasing characteristics of laser-driven potassium atoms contained in a high-finesse optical resonator. (a) Laser intensity β^2 vs cavity detuning Δ_c for $\kappa=0.05$ and for different values of drive amplitude. (b) Laser intensity vs cavity detuning Δ_c for different values of the unsaturated gain parameter g and $\alpha=15$ and $\kappa=0.15$. From left to right, the values of g are 3000, 2900, 2800, 2700, 2600, 2500, 2400, and 2300. (c) Laser intensity vs cavity losses κ for different drive amplitudes α with $\Delta_c=9.2$ and $g=3000$. The rest of the parameters as in previous figures.

We now focus on those cases of low or moderate drive amplitudes or large cavity losses to characterize in greater detail the (2+2) multiphoton stable emission. Figure 8 shows the influence of several laser parameters on the emission. Figure 8(a) shows the influence of the drive amplitude, where lasing only occurs for α ranging between 9.4 and 15.

No time-dependent emission branch connected with the represented stable branch has been found. It can be seen that increasing the drive amplitude increases the laser emission intensity and widens the range of cavity-detuning values where (2+2) multiphoton lasing occurs. There is a point, however, where further increase of the drive amplitude does not increase the stable emission intensity nor the cavity detuning range (the cavity detuning range decreases and blueshifts). This occurs roughly at the same value of the drive amplitude at which the (4+3) processes start to influence the highest-intensity part of the stable emission branch (see the distortion of the upper wing of the curves due to such processes).

Figure 8(b) shows the influence of the unsaturated gain parameter g (proportional to the number of atoms in the cavity) on the stable (2+2) emission branch. Clearly, decreasing the unsaturated gain parameter decreases almost linearly the maximum emission intensity. The cavity detuning range also decreases. In some cases, the upper extreme point of the branch connects with a short branch where the emission intensity is slightly modulated in time.

Finally, Fig. 8(c) shows the dependence of the (2+2) stable laser emission intensity on the cavity losses. As it can be seen, increasing the cavity losses strongly decreases the emission intensity. Beyond the extreme points of each branch, laser emission disappears.

B. $\Sigma_n(n+n)$ multiphoton laser emission

Another interesting process is $\Sigma_n(n+n)$ multiphoton lasing, which is shown schematically in Fig. 9(a). When this process is on resonance with atomic states $|g,2,M\rangle$ (i.e., with $F=2$ states in the ground manifold), it occurs simultaneously for all M states in this manifold so that the final state can be any one of these states (or, alternatively, such a final state can be regarded as a coherent superposition of all these atomic states). Thus, this global process can be described as a superposition of "Rayleigh" and "hyper-Rayleigh" processes (1+1), and (2+2), and (3+3), and (4+4), and combinations of these process. Such a global process could thus be potentially useful to transfer efficiently and in a controlled way population from the initial atomic state to any of these final states, which would entail a change in the z projection of the atomic angular momentum. It could also be useful to generate multiphoton correlated field states. Details of the amplification characteristics of these processes were given in Ref. [28], although states with $M=-2$ were neglected. Here we provide more accurate results about the amplification process and describe new results about lasing and population transfers.

Figure 9(b) shows the multiphoton gain as a function of the laser field detuning Δ_L, for a fixed drive amplitude and several values of the probe (or lasing) field amplitude β. The observed behavior can be interpreted as follows. For low lasing amplitudes, only the initial step of the global multiphoton process plays a significant role [i.e., the (1+1) process, which arises from single-photon lasing with regards to the probe field]. Our interpretation is supported by the fact that the maximum gain occurs for low probe amplitude (it occurs for $\beta \to 0$), which is a well-known characteristic of single-photon processes. For increasing laser intensity, there is an increasing contribution from the higher-order quantum processes; first the (2+2) process, then the (3+3) process and finally the (4+4) process. This is supported by the fact that the saturation of the gain peak when the lasing amplitude β is increased (which manifests in the form of gain-peak reduction and broadening) is smaller than in the case of a pure (1+1) process. We have checked this point by repeating the calculations of Fig. 9(b) ignoring in the numerical code the presence of all the atomic states with M smaller than 1. For such an hypothetical case, we have observed that the gain-peak reduction is larger than in Fig. 9(b) when β is increased, for instance, from $0.01 \to 1 \to 12 \to 20$, by factors 1.4, 2.9, and 1.1, respectively; at the same time, this larger

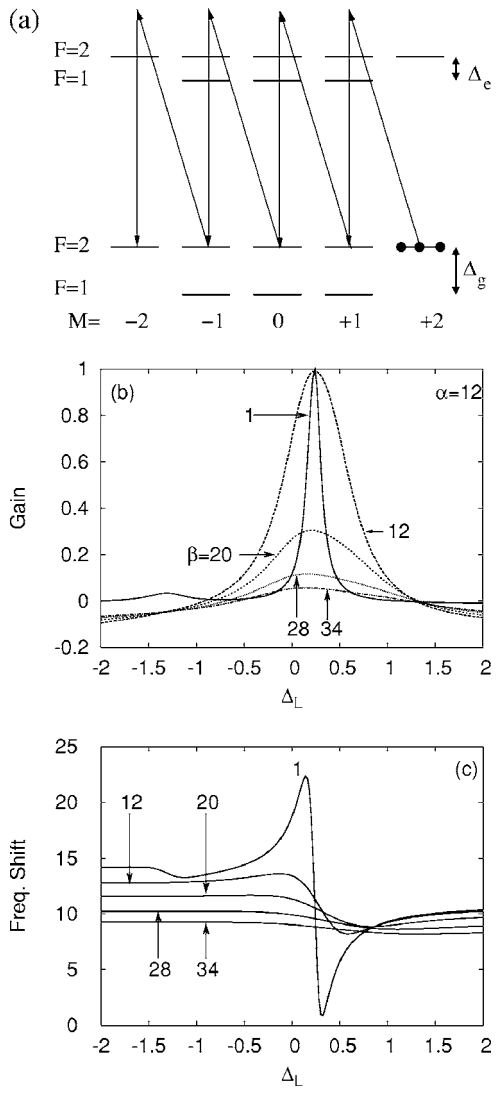

FIG. 9. Characteristics of the $\Sigma_n(n+n)$ amplification process. (a) Multiphoton process starting at atomic state $|g,2,2\rangle$. (b) Gain vs laser field detuning Δ_L for $\alpha=12$ and several values of the probe amplitude. The curve corresponding to $\beta=1$ has been divided by 20 for clarity; the gain peak for $\beta \to 0$ is only 10% higher than for $\beta=1$. (c) Frequency shift vs laser field detuning Δ_L for the same parameters as in (b).

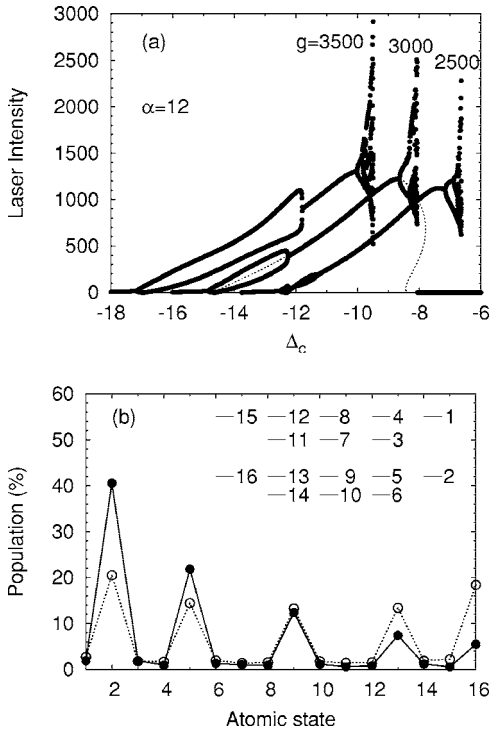

FIG. 10. Characteristics of $\Sigma_n(n+n)$ lasing. (a) Laser intensity β^2 vs cavity detuning Δ_c for $\alpha=12$ and different values of the unsaturated gain g: from left to right $g=3500$, 3000, and 2500 (other parameters as in Fig. 2). (b) Population (as a percentage) that accumulates at each atomic state for $g=3000$ and $\Delta_c=-12$ (thick line, solid circles) and $\Delta_c=-8.7$ (dashed line, open circles). The atomic state labeling is the same as in Fig. 6.

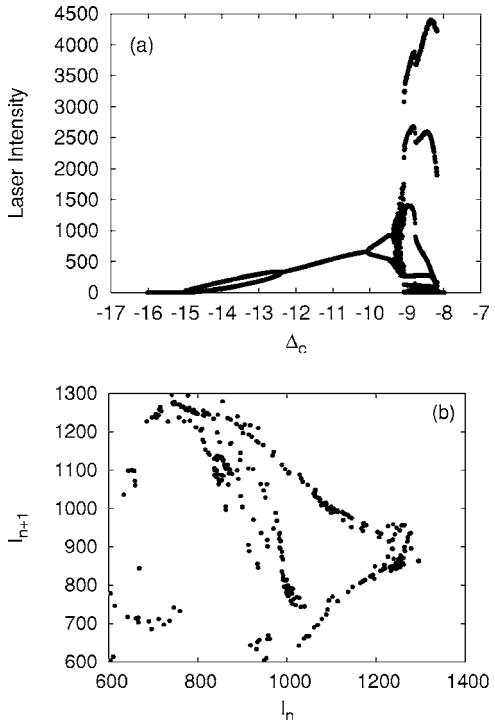

FIG. 11. Characteristics of $\Sigma_n(n+n)$ lasing for higher cavity losses. (a) Maxima and minima laser intensity vs cavity detuning Δ_c for $\alpha=12$, $\kappa=0.15$, repopulation rate $\gamma_{out}=0.07$ and $g=3000$. The dominant process of laser emission is a Rayleigh multiphoton process involving two, four, six, and eight photons. (b) Intensity return map for a cavity detuning $\Delta_c=-9.25$, and the rest of the parameters as in the previous figure.

peak reduction is accompanied by a larger gain-peak broadening. The increasing participation of the higher-order multiphoton processes partially counterbalances saturation of the $(1+1)$ process (but never overtakes it). We have checked that such kinds of behavior also holds for smaller values of the drive amplitude α, although it can be difficult to observe when α is much less than 1.

Figure 9(c) shows the frequency shifts associated to the gain curves shown in Fig. 9(b). The saturation also affects significantly these dispersive profiles. Note that the average value of the frequency shift for this process is larger than in the case of the $(2+2)$ processes analyzed above.

The $\Sigma_n(n+n)$ lasing characteristics are shown in Fig. 10(a). In contrast with $(2+2)$ lasing, it is seen here that the stationary emission curve obtained using strategy (i) (thin dotted line—shown only for $g=3000$ for the sake of clarity) is in contact with both ends with the zero-intensity branch through local bifurcations (see below). Following strategy (ii) (thick line), it is seen that the laser displays both stable emission, indicated by a single valued curve, or time-dependent behavior, indicated by a multivalued curve where both the maxima and the minima of the laser intensity along time evolution have been plotted. It can be seen that the stable laser emission branch undergoes a Hopf bifurcation close to the laser emission threshold, which introduces a periodic modulation of the output intensity. Upon increasing cavity detuning, the laser intensity monotonically increases. A relatively large domain of stable emission is found, which eventually ends with a bifurcation that is the beginning of a route to a narrow domain of chaos. Beyond the chaotic domain, laser emission disappears. For decreasing values of the unsaturated gain g, the domain of stable emission rapidly increases at the expense of the first domain of periodic behavior.

Figure 10(b) shows the populations that accumulate in each of the atomic states for two specific points of the laser emission branch depicted in Fig. 10(a). The laser emission intensity is stable and relatively low (unstable and relatively high) for the case shown by solid circles (open circles). It can be seen in both cases that the population is transferred significantly from the initial atomic state $|g,2,2\rangle$ to only the "on-resonance" atomic states $|g,2,M\rangle$, for any value of M. The most remarkable feature of this plot is that this transfer is very large to any of these states, especially to those with a value of M far from the initial value $M=2$; namely, to states with $M=-2$ and -1. This occurs more dramatically in the second case (open circles, dashed line), for which the population of state $|g,2,-2\rangle$ is almost the same as that of the initial state $|g,2,2\rangle$. This means that the resonant "hyper-Rayleigh" processes considered here can be very efficient for rapidly transferring the population from certain ground states to other ground states involving large changes in the z component of the atomic angular momentum.

Figure 11(a), which is similar to Fig. 10(a) but for cavity

losses three times larger, shows that in this case, increasing the cavity losses does not lead to a significant simplification of the laser emission behavior (in contrast with what is observed, for instance, in Fig. 5 above). The domain of periodic emission near threshold persists, and the domain of chaotic emission at large a intensity also persists, with huge intensity spikes. This is in contrast with what has been found above for the (2+2) laser emission, where increasing the cavity losses ensured more regular and stable behavior. Figure 11(b) shows an intensity return map for a value of the cavity detuning corresponding to the chaotic region of Fig. 11(a), where it is seen that the behavior is of rather high dimension (not described by a simple one-dimensional return map).

C. Other multiphoton lasing processes

As seen in the wide laser emission spectrum of Fig. 2(b), there exist additional resonances brought about by other multiphoton processes. The most important ones are those corresponding to the Raman (1+1) process connecting the initial atomic state $|g,2,2\rangle$ with the final state $|g,1,1\rangle$ and to (2+1) processes connecting the initial state $|g,2,2\rangle$ with final states $|e,2,0\rangle$ or $|e,1,0\rangle$. The gain characteristics associated with these multiphoton processes were already discussed in Ref. [28], although the lasing characteristics were not investigated. Finally, other lasing resonances, barely noticeable in Fig. 2(b), are those appearing at $\Delta_c \approx -1$ and $\Delta_c \approx 3$. They can be attributed to (2+1) processes starting both at atomic state $|g,1,1\rangle$ and ending at states $|e,2,-1\rangle$ and $|e,1,-1\rangle$, respectively. Note that state $|g,1,1\rangle$ is populated via spontaneous emission decay from excited levels, in particular, from level $|e,2,1\rangle$, as well as by transfer from the initial state $|g,2,2\rangle$ due to the (1+1) Raman process pointed out above. It is also worth noting that only lasing resonances including only multiphoton processes $(n+m)$ with m larger than 1 are disconnected from and coexist with the zero-intensity solution branch.

From Fig. 2(b), it is seen that the largest laser emission intensities are obtained by the highest-order multiphoton processes rather than the lowest. This is because high-order multiphoton processes have a larger saturation threshold even if their emission threshold is higher than in the case of the low-order processes. This might be useful for certain applications.

IV. CONCLUSIONS

In conclusion, we have developed an accurate model of n-photon lasing occurring when laser-driven ^{39}K are placed in a high-finesse optical cavity as investigated experimentally by Pfister *et al.* [29,25]. The richness of the degenerate magnetic sublevels of the D_1 transition gives rise to a wide variety of multiphoton lasing, including two-photon lasing and degenerate n-photon lasing. Future theoretical investigations are needed to account for the polarization instabilities observed in Ref. [25]. We hope that our exploration of n-photon lasing will spur additional experiments because of the possibility of generating high-order correlated states of the electromagnetic field.

[1] D. J. Gauthier, *Progress in Optics* (Elsevier, North Holland, 2003), Vol. 45.
[2] K. McNeil and D. Walls, J. Phys. A **8**, 104 (1975).
[3] L. Sczaniecki, Opt. Acta **27**, 251 (1980).
[4] M. Reid, K. J. McNeil, and D. F. Walls, Phys. Rev. A **24**, 2029 (1981).
[5] U. Herzog, Opt. Acta **30**, 639 (1983).
[6] A. Bandilla and H. Voigt, Z. Phys. B: Condens. Matter **58**, 165 (1985).
[7] F. L. Li, D. L. Lin, T. F. George, and X. S. Li, Phys. Rev. A **40**, 1394 (1989).
[8] M. Abdalla, M. Ahmed, and A. Obada, Physica A **162**, 215 (1990).
[9] M. H. Mahran and A. S. F. Obada, Phys. Rev. A **42**, 1718 (1990).
[10] T. Magbool and M. S. K. Razmi, Phys. Rev. A **44**, 6147 (1991).
[11] C. Sukumar and B. Buck, Phys. Lett., C **83**, 211 (1991).
[12] A. Rosenhouse-Dantsker, J. Mod. Opt. **39**, 147 (1992).
[13] H. X. Meng, J. L. Chai, and Z. M. Zhang, Phys. Rev. A **45**, 2131 (1992).
[14] M. Fang and P. Zhou, J. Mod. Opt. **42**, 1199 (1995).
[15] K. Matsuo and H. Iwasawa, Jpn. J. Appl. Phys., Part 1 **35**, 613 (1996).
[16] N. Enaki and V. Koroli, J. Phys. B **31**, 3583 (1998).
[17] N. Abdel-Wahab, Phys. Scr. **71**, 132 (1983).
[18] B. Nikolaus, D. Z. Zhang, and P. E. Toschek, Phys. Rev. Lett. **47**, 171 (1981).
[19] J. Sparbier, K. J. Boller, and P. E. Toschek, Appl. Phys. B **62**, 227 (1996).
[20] D. J. Gauthier, Q. Wu, S. E. Morin, and T. W. Mossberg, Phys. Rev. Lett. **68**, 464 (1992).
[21] J. Zakrezewski, M. Lewenstein, and T. W. Mossberg, Phys. Rev. A **44**, 7717 (1991).
[22] J. Zakrezewski, M. Lewenstein, and T. W. Mossberg, Phys. Rev. A **44**, 7732 (1991).
[23] J. Zakrezewski, M. Lewenstein, and T. W. Mossberg, Phys. Rev. A **44**, 7746 (1991).
[24] J. Zakrzewski and M. Lewenstein, Phys. Rev. A **45**, 2057 (1992).
[25] O. Pfister, W. J. Brown, M. D. Stenner, and D. J. Gauthier, Phys. Rev. Lett. **86**, 4512 (2001).
[26] A. Kulminskii, D. J. Gauthier, R. Vilaseca, J. J. Fernández-Soler, and J. L. Font, J. Opt. B: Quantum Semiclassical Opt. **5**, 243 (2003).
[27] J. J. Fernández-Soler, J. L. Font, R. Vilaseca, D. J. Gauthier, A. Kul'minskii, and O. Pfister, Phys. Rev. A **65**, 031803 (2002).
[28] J. J. Fernández-Soler, J. L. Font, R. Vilaseca, D. J. Gauthier, and A. Kul'minskii, Phys. Rev. A **68**, 043824 (2003).

[29] O. Pfister, W. J. Brown, M. D. Stenner, and D. J. Gauthier, Phys. Rev. A **60**, R4249 (1999).
[30] C. Weiss and R. Vilaseca, *Dynamics of Lasers* (VCH, Weinheim, 1991).
[31] P. Mandel, *Theoretical Problems in Cavity Nonlinear Optics* (Cambridge University Press, Cambridge, 1997).
[32] Y. Khanin, *Principles of Laser Dynamics* (North-Holland, Amsterdam, 1995).
[33] G. J. de Valcárcel, E. Roldán, J. F. Urchueguía, and R. Vilaseca, Phys. Rev. A **52**, 4059 (1995).